HOKKAIDO UNIVERSITY

Title	Anomaly Detection in Each Modal Response Using Bayesian Hypothesis Testing and Stochastic Subspace Identification
Author(s)	Goi, Yoshinao
Relation	Proceedings of the 10th International Symposium on Reliability Engineering and Risk Management (ISRERM 2026), June 28 - July 1, 2026, Sapporo, Japan
Citation	Proceedings of the 10th International Symposium on Reliability Engineering and Risk Management (ISRERM 2026)
Issue Date	2026-07-01
Doc URL	https://hdl.handle.net/2115/100474
Type	conference paper
File Information	C000247_1.pdf

Hokkaido University Collection of Scholarly and Academic Papers : HUSCAP

10th International Symposium on Reliability Engineering and Risk Management (ISRERM 2026),
28 June-01 July 2026, Sapporo, Japan
Kitahara, T., Miyamori, Y. & Beer, M. (editors)

Anomaly Detection in Each Modal Response Using Bayesian Hypothesis Testing and Stochastic Subspace Identification

Yoshinao Goi[1] *

[1]*Department of Civil Engineering, Faculty of Engineering, Gifu University, Address, Japan.*
E-mail: goi.yoshinao.p3@f.gifu-u.ac.jp
**Corresponding Author*

This study proposes a two-step anomaly-detection method for the upper structures of bridges using vehicle-induced vibration acceleration. The first step trains a structural model from the reference dataset. Bayesian inference is applied to a vector autoregressive (VAR) model. The autoregressive order is automatically adjusted with the Bayesian information criterion. Covariance-driven stochastic subspace identification (SSI-COV) is applied to find the damage-sensitive parametric subspace in which the parameters represent modal properties in the trained model. The dimension of the parametric subspace is adjusted by the signal-to-noise ratio, comparing the power of each modal response to the noise. The second step detects anomalies by comparing the test dataset to the trained model. Bayesian hypothesis testing is applied to detect changes in the parametric subspace. SSI-COV enables anomaly detection in each modal property directly from measured acceleration. Therefore, we can expect the proposed method to shorten the screening process before further analysis. A field experiment on a truss bridge with severed members was examined as a case study.

Keywords: Structural health monitoring, Change detection, Modal properties, Stochastic subspace identification, Bayesian hypothesis testing

1 Introduction

Among the various vibration-based anomaly detection methods for bridge upper structures, most previous studies have focused on changes in modal properties, such as modal frequencies, modal shapes, damping ratios, and related parameters (Rabi et al., 2024). That is because changes in the stiffness of the primary members cause changes in the modal properties of the whole structure. Therefore, in most studies, estimating and comparing the modal properties are required to find their changes. However, to automate the comparison procedure, engineers need to put in additional effort to distinguish statistically significant changes from the modal property estimators. Especially under noisy conditions, such as vehicle-induced vibration, the feature extraction procedure requires adjusting thresholds in signal processing.

For screening numerous bridges, automated signal processing for change detection in modal properties is desired. Aiming at automated processing, the authors previously proposed a Bayesian hypothesis testing method (Goi & Kim, 2023). In this method, Bayesian inference is applied to a vector autoregressive (VAR) model to represent bridge vibration. Bayesian hypothesis testing quantifies anomalies in a subspace extracted with principal component analysis. Although the previous study enables prompt screening for change detection, the result indicates only that modal properties are somehow altered. To find which mode is altered, further investigation is needed after applying the previous method.

This study uses covariance-driven stochastic subspace identification (SSI-COV) rather than principal component analysis for feature extraction. The primary advantage of the proposed method in this study is accountability through the well-known modal identification method. SSI-COV enables automating the estimation of modal properties from the reference dataset and directly detecting anomalies in each modal property from measured acceleration. A field experiment on a truss bridge with severed members (Kim et al., 2021) was examined as a case study.

2 Proposed method

2.1 *Bayesian inference for the VAR model*

Let a synchronized *m*-DOF time series of the acceleration be measured on a bridge. A zero-mean time series is produced by subtracting the mean value from the measured acceleration. Let $\boldsymbol{y}_k \in \mathbb{R}^{m\times 1}$ $(k = 1 \ldots n)$ denote a column vector at the *k*-th time step of the zero-mean time series with components corresponding to the measurement locations. The following VAR model with AR coefficient matrices $\boldsymbol{\alpha}_i \in \mathbb{R}^{m\times m}$ and sufficient numbers of model order p approximates the acceleration response.

$$\boldsymbol{y}_k = \sum_{i=1}^{p} \boldsymbol{\alpha}_i \boldsymbol{y}_{k-i} + \boldsymbol{e}_k \ = \mathbf{W}\boldsymbol{\phi}_k + \boldsymbol{e}_k (\text{for } k = p+1, \ldots, n) \tag{1}$$

where $\mathbf{W} = [\boldsymbol{\alpha}_p, \ldots, \boldsymbol{\alpha}_1] \in \mathbb{R}^{m\times mp}$, and $\boldsymbol{\phi}_k = \left[\boldsymbol{y}_{k-p}^{\mathrm{T}}, \ldots, \boldsymbol{y}_{k-1}^{\mathrm{T}}\right]^{\mathrm{T}} \in \mathbb{R}^{mp\times 1}$. To describe the covariance-driven method, the autocorrelation function is defined as follows for the infinite sequence $[\boldsymbol{y}_1, \boldsymbol{y}_2, \ldots]$.

$$\mathbf{R}(s) = \mathbb{E}_k\left[\boldsymbol{y}_k \boldsymbol{y}_{k-s}^{\mathrm{T}}\right] = \lim_{N\to\infty} \frac{1}{N} \sum_{k=1}^{N} \boldsymbol{y}_k \boldsymbol{y}_{k-s}^{\mathrm{T}} \tag{2}$$

Let l sets of finite time series of acceleration be acquired as the reference dataset: $\mathbf{Y}_i = \left[\boldsymbol{y}_1^{i\mathrm{T}}, \dots, \boldsymbol{y}_{n_i}^{i\mathrm{T}}\right]^{\mathrm{T}} (i = 1 \dots l)$ stands for each of the time series where n_i $(i = 1 \dots l)$ is its data length. Let $\mathcal{D}_{\mathrm{r}}$ represent the reference dataset as $\mathcal{D}_{\mathrm{r}} = \{\mathbf{Y}_1 \dots \mathbf{Y}_l\}$, where the subscript "r" denotes "reference." For whole reference dataset, the estimator of the auto correlation functions is obtained as

$$\widehat{\mathbf{R}}_{\mathrm{r}}(s) = \begin{cases} \frac{1}{N} \Sigma_{i=1}^{l} \Sigma_{k=s+1}^{n_i} \left(\boldsymbol{y}_k^i \boldsymbol{y}_{k-s}^{i\mathrm{T}}\right) & (\text{for } s \geq 0) \\ \widehat{\mathbf{R}}_{\mathrm{r}}(s)^{\mathrm{T}} & (\text{for } s < 0) \end{cases} \tag{3}$$

Here, N represents the total data length of the reference dataset, i.e., $N = \Sigma_{i=1}^{l} n_i$. In this study, we assume that the approximation $\mathbf{R}(s) \approx \widehat{\mathbf{R}}_{\mathrm{r}}(s)$ holds for the reference dataset.

Let $\mathbf{T}_{\mathbf{r}}(s)$ be $mp \times mp$ Block Toeplitz matrix for the reference dataset as

$$\mathbf{T}_{\mathbf{r}}(s) = \begin{bmatrix} \widehat{\mathbf{R}}_{\mathrm{r}}(s) & \dots & \widehat{\mathbf{R}}_{\mathrm{r}}(s-p+1) \\ \vdots & \ddots & \vdots \\ \widehat{\mathbf{R}}_{\mathrm{r}}(s+p-1) & \dots & \widehat{\mathbf{R}}_{\mathrm{r}}(s) \end{bmatrix} \tag{4}$$

Bayes' theorem with a non-informative prior yields the following conditional probability density function (PDF).

$$\wp(\mathbf{W}, \boldsymbol{\Sigma} | \mathcal{D}_{\mathrm{r}}) = \mathcal{MN}(\mathbf{W} | \mathbf{M}, \boldsymbol{\Sigma}, \mathbf{L}^{-1}) \mathcal{IW}(\boldsymbol{\Sigma} | \boldsymbol{\Psi}, \nu), \tag{5}$$

Therein, $\wp(\cdot \mid \cdot)$ represent conditional PDF, and $\mathcal{MN}(\mathbf{W}|\mathbf{M}, \boldsymbol{\Sigma}, \mathbf{L}^{-1})$ and $\mathcal{IW}(\boldsymbol{\Sigma}|\boldsymbol{\Psi}, \nu)$ stand respectively for the matrix-normal and inverse-Wishart distributions as

$$\mathcal{MN}(\mathbf{W}|\mathbf{M}, \boldsymbol{\Sigma}, \mathbf{L}^{-1}) = (2\pi)^{-\frac{m^2 p}{2}} |\mathbf{L}^{-1}|^{-\frac{m}{2}} |\boldsymbol{\Sigma}|^{-\frac{mp}{2}} \exp\left\{-\frac{1}{2} \mathrm{tr}[\mathbf{L}(\mathbf{W}-\mathbf{M})^{\mathrm{T}} \boldsymbol{\Sigma}^{-1} (\mathbf{W}-\mathbf{M})]\right\} \tag{5}$$

$$\mathcal{IW}(\boldsymbol{\Sigma}|\boldsymbol{\Psi}, \nu) = 2^{-\frac{\nu m}{2}} \Gamma_m\left(\frac{\nu}{2}\right) |\boldsymbol{\Psi}|^{\frac{\nu}{2}} |\boldsymbol{\Sigma}|^{-\frac{(\nu+m+1)}{2}} \exp\left\{-\frac{1}{2} \mathrm{tr}[\boldsymbol{\Psi}\boldsymbol{\Sigma}^{-1}]\right\}, \tag{6}$$

Here, each hyperparameter is calculated as

$$\nu = \sum_{i=1}^{l} (n_i - p), \qquad \mathbf{L} = \nu \mathbf{T}_{\mathrm{r}}(0), \qquad \mathbf{M} = \left[\widehat{\mathbf{R}}_{\mathrm{r}}(p) \dots \widehat{\mathbf{R}}_{\mathrm{r}}(1)\right] \mathbf{T}_{\mathrm{r}}(0)^{-1}, \qquad \boldsymbol{\Psi} = \nu \widehat{\mathbf{R}}_{\mathrm{r}}(0) - \mathbf{M}\mathbf{L}\mathbf{M}^{\mathbf{T}} \tag{7}$$

To find an appropriate AR order p, the following Bayesian information criterion (BIC) is adopted.

$$BIC = \nu \ln \left|\frac{\boldsymbol{\Psi}}{\nu}\right| + \left(m^2 p + \frac{m(m+1)}{2}\right) \ln \nu\,. \tag{8}$$

Hereinafter, we apply the BIC to optimize the AR order p.

2.2 *Covariance-driven stochastic subspace identification*

SSI for an output-only system is formulated as the following state-space model.

$$\boldsymbol{x}_{k+1} = \mathbf{A}\boldsymbol{x}_k + \boldsymbol{w}_k \tag{9}$$

$$\boldsymbol{y}_k = \mathbf{C}\boldsymbol{x}_k + \boldsymbol{v}_k \tag{10}$$

Let q be the DOF of the modeled equation of motion, the dimension of the state vector $\boldsymbol{x}_k$ is known to be $2q$. The constant matrices $\mathbf{A} \in \mathbb{R}^{2q \times 2q}$ and $\mathbf{C} \in \mathbb{R}^{m \times 2q}$ relate to modal properties of the bridge, $\boldsymbol{w}_k$ and $\boldsymbol{v}_k$ are the noise terms. This study assumes the reference dataset generated by the state-space model described above. After p-step filtering by the non-steady state Kalman filter, the one-step-ahead prediction of the state vector $\widehat{\boldsymbol{x}}_k$ is given as

$$\widehat{\boldsymbol{x}}_k = \boldsymbol{\Delta}\, \mathbf{T}_{\mathrm{r}}(0)^{-1} \boldsymbol{\phi}_k \tag{11}$$

Herein, $\boldsymbol{\Delta}$ is the following controllability matrix

$$\boldsymbol{\Delta} = [\mathbf{G}\ \mathbf{A}\mathbf{G}\ \dots\ \mathbf{A}^{p-1}\mathbf{G}], \qquad \mathbf{G} = \mathbb{E}[\boldsymbol{x}_{k+1} \boldsymbol{y}_k^{\mathrm{T}}] \tag{12}$$

On the other hand, the following relationship is known.

$$\mathbf{T}_{\mathrm{r}}(p) = \boldsymbol{\Gamma}\boldsymbol{\Delta} \tag{13}$$

Herein, $\boldsymbol{\Gamma}$ is the following observability matrix.

$$\boldsymbol{\Gamma} = \begin{bmatrix} \mathbf{C} \\ \mathbf{C}\mathbf{A} \\ \vdots \\ \mathbf{C}\mathbf{A}^{p-1} \end{bmatrix} \tag{14}$$

Typically, SSI-COV applies SVD to the Toeplitz matrix $\mathbf{H}(p)$. However, this study applies the unweighted principal component (UPC) algorithm (van Overschee & De Moor, 1996) to ensure theoretical consistency of the proposed hypothesis testing. In UPC, the observability matrix is determined from the range of the left singular vectors of $\mathbf{T}_{\mathbf{r}}(p)\ \mathbf{T}_{\mathbf{r}}(0)^{-1}\mathbf{T}_{\mathbf{r}}(p)$. Using the autocorrelation functions estimated from the reference dataset, the following SVD yields the singular vectors for UPC.

$$\mathbf{T}_{\mathbf{r}}(p)\mathbf{T}_{\mathrm{r}}(0)^{-1/2} = \mathbf{U}\mathbf{S}\mathbf{V}^{\mathrm{T}} = [\mathbf{U}_{\mathbf{I}} \quad \mathbf{U}_{\mathbf{II}}] \begin{bmatrix} \mathbf{S}_{\mathbf{I}} & \mathbf{O} \\ \mathbf{O} & \mathbf{S}_{\mathbf{II}} \end{bmatrix} \begin{bmatrix} \mathbf{V}_{\mathbf{I}}^{\mathrm{T}} \\ \mathbf{V}_{\mathbf{II}}^{\mathrm{T}} \end{bmatrix} \tag{15}$$

Here, $\mathbf{U_I}$, $\mathbf{S_I}$ and $\mathbf{V_I}$ represent submatrices composed of the first $2q$ singular vectors and singular values, and $\mathbf{U_{II}}$, $\mathbf{S_{II}}$ and $\mathbf{V_{II}}$ are the latter part. In SSI, we assume the higher-order singular values in $\mathbf{S_{II}}$ are almost zero. Equation 13 produces the observability matrix and controllability matrix estimators as

$$\mathbf{\Gamma} = \mathbf{U_I}\mathbf{S_I^{1/2}}, \qquad \mathbf{\Delta} = \mathbf{S_I^{1/2}}\mathbf{V_I^{\mathrm{T}}}\mathbf{T}_{\mathrm{r}}(0)^{1/2} \tag{16}$$

Matrices $\mathbf{A}$ and $\mathbf{C}$ are estimated from Equations 14 and 16.

Using linear transform $\mathbf{Q} = \widehat{\mathbf{T}}_{\mathrm{r}}(0)^{1/2}\mathbf{V}\mathbf{S^{-1/2}}$, its submatrices $\mathbf{Q_I} = \widehat{\mathbf{T}}_{\mathrm{r}}(0)^{1/2}\mathbf{V_I}\mathbf{S_I^{-1/2}}$ and $\mathbf{Q_{II}} = \widehat{\mathbf{T}}_{\mathrm{r}}(0)^{1/2}\mathbf{V_{II}}\mathbf{S_{II}^{-1/2}}$, let parametric subspace on $\mathbf{W}$ be split as $\widetilde{\mathbf{W}} = \mathbf{WQ} = [\mathbf{WQ_I} \quad \mathbf{WQ_{II}}] = [\widetilde{\mathbf{W}}_{\mathrm{I}} \quad \widetilde{\mathbf{W}}_{\mathrm{II}}]$. Then the following approximation satisfies.

$$\mathbf{Q^{-1}}\boldsymbol{\phi}_k \approx \begin{bmatrix} \mathbf{\Delta}\,\mathbf{T}_{\mathrm{r}}(0)^{-1}\boldsymbol{\phi}_k \\ \mathbf{0} \end{bmatrix} = \begin{bmatrix} \widehat{\boldsymbol{x}}_k \\ \mathbf{0} \end{bmatrix} \tag{17}$$

Equations 7 and 13 to 16 show that the most probable value of $\widetilde{\mathbf{W}}_{\mathrm{I}}$ in Equation 5 corresponds to the estimator of $\mathbf{C}$. Accordingly,

$$\boldsymbol{y}_k = \mathbf{W}\boldsymbol{\phi}_k + \boldsymbol{e}_k = \mathbf{WQQ^{-1}}\boldsymbol{\phi}_k + \boldsymbol{e}_k \approx \mathbf{C}\widehat{\boldsymbol{x}}_k + \boldsymbol{e}_k \tag{18}$$

The above relation states that the VAR model corresponds to one-step-ahead estimation in a state-space model under the SSI assumption.

The signal-to-noise (S/N) ratio of the total observed modal response for q DOF is given as

$$\mathrm{SN}_{\mathrm{Total}}(q) = \frac{\mathbf{tr}\left[\mathbb{E}_k[(\mathbf{C}\widehat{\boldsymbol{x}}_k)(\mathbf{C}\widehat{\boldsymbol{x}}_k)^{\boldsymbol{T}}]\right]}{\mathbf{tr}\left[\mathbb{E}_k[\boldsymbol{e}_k\boldsymbol{e}_k^T]\right]} = \frac{\mathbf{tr}[\mathbf{CS_IC^T}]}{\mathbf{tr}[\mathbf{\Sigma}]} = \frac{\mathbf{tr}[\mathbf{CS_IC^T}]}{\mathbf{tr}[\mathbf{\Sigma}]} \tag{19}$$

This study proposes to automate adjusting the DOF q by the following differential SN ratio as

$$\mathrm{SN}_{\mathrm{Diff}}(q) = \mathrm{SN}_{\mathrm{Total}}(q) - \mathrm{SN}_{\mathrm{Total}}(q-1) \tag{20}$$

When $\mathrm{SN}_{\mathrm{Diff}}(q) > 1$, the q-th DOF is physically meaningful. Therefore, this study adopts the q that satisfies $\mathrm{SN}_{\mathrm{Diff}}(q) > 1$.

2.3 *Change detection for each modal response*

Let the principal component decomposition of $\mathbf{A}$ be

$$\mathbf{A} = \mathbf{P\Lambda P^{-1}} = [\boldsymbol{p_1} \quad \boldsymbol{p_1^*} \quad \dots \quad \boldsymbol{p}_q \quad \boldsymbol{p}_q^*]\mathrm{diag}[\lambda_1 \quad \lambda_1^* \quad \dots \quad \lambda_q \quad \lambda_q^*][\boldsymbol{p_1^-} \quad \boldsymbol{p_1^{-*}} \quad \dots \quad \boldsymbol{p}_q^- \quad \boldsymbol{p}_q^{-*}]^{\mathrm{T}} \tag{21}$$

Hear, the scalar $\lambda_1, \dots, \lambda_q$ are the pole of the state space model and their conjugate pair, the mode vectors $\boldsymbol{p_1}, \dots, \boldsymbol{p}_q$ and $\boldsymbol{p_1^-}, \dots, \boldsymbol{p}_q^-$ are the corresponding right and left eigen vectors. " * " represents their conjugate pairs. Note that each of the poles and the mode vectors represents a modal response in the state equation. Letting $\widetilde{\mathbf{W}}'_{\mathbf{I},\boldsymbol{i}} = \sqrt{\mathbf{2}}\widetilde{\mathbf{W}}_{\mathrm{I}}[\mathrm{re}(\boldsymbol{p_i}) \quad \mathrm{im}(\boldsymbol{p_i})]$ and $\widetilde{\mathbf{W}}' = \left[\underset{q}{\widetilde{\mathbf{W}}'_{\mathbf{I},\mathbf{1}}}, \dots \; \widetilde{\mathbf{W}}'_{\mathbf{I},\boldsymbol{q}}, \quad \widetilde{\mathbf{W}}_{\mathrm{II}}\right]$, Equation 5 can be rewritten as

$$p\left(\widetilde{\mathbf{W}}', \mathbf{\Sigma}|\mathcal{D}_{\mathrm{r}}\right) = \prod_{i=1}^{} \mathcal{MN}\left(\widetilde{\mathbf{W}}'_{\mathbf{I},i}|\widetilde{\mathbf{M}}'_{\mathbf{I},i}, \mathbf{\Sigma}, \tilde{\mathbf{L}}_{\mathbf{I},i}^{-\mathbf{1}}\right) \times \mathcal{MN}\left(\widetilde{\mathbf{W}}_{\mathrm{II}}|\widetilde{\mathbf{M}}_{\mathrm{II}}, \mathbf{\Sigma}, \tilde{\mathbf{L}}_{\mathbf{II}}^{-\mathbf{1}}\right)\mathcal{IW}(\mathbf{\Sigma}|\mathbf{\Psi}, \nu) \tag{22}$$

where

$$\tilde{\mathbf{L}}'_{\mathbf{I},\boldsymbol{i}} = 2\nu\begin{bmatrix} \mathrm{re}(\boldsymbol{p}_i^-)^{\mathrm{T}}\mathbf{S_I}\mathrm{re}(\boldsymbol{p}_i^-) & 0 \\ 0 & \mathrm{im}(\boldsymbol{p}_i^-)^{\mathrm{T}}\mathbf{S_I}\mathrm{im}(\boldsymbol{p}_i^-) \end{bmatrix}, \qquad \tilde{\mathbf{L}}_{\mathbf{II}} = \nu\mathbf{S_{II}} \tag{23}$$

$$\widetilde{\mathbf{M}}'_{\mathbf{I},\boldsymbol{i}} = \sqrt{\mathbf{2}}\mathbf{MQ_I}[\mathrm{re}(\boldsymbol{p_i}) \quad \mathrm{im}(\boldsymbol{p_i})], \qquad \widetilde{\mathbf{M}}_{\mathbf{II}} = \mathbf{MQ_{II}} \tag{24}$$

This study adopts two statistical models, one representing the healthy bridge and the other the damaged bridge. Following the hypothesis testing precedent, the healthy and damaged bridge models are designated as the "null hypothesis" and the "alternative hypothesis." Let $\mathcal{D}_{\mathrm{t}}$ denote the test dataset for the hypothesis testing. Herein, subscript "t" stands for "test."

Let $\mathbf{\Theta}$ represent the set of the regressive parameters. Let $\mathbf{\Theta}_{\mathrm{feat}} \in \mathbf{\Theta}$ represent the damage-sensitive parameters. For hypothesis testing, let $\mathbf{\Theta}_{\mathrm{feat}}^{\mathrm{r}}$ and $\mathbf{\Theta}_{\mathrm{feat}}^{\mathrm{t}}$ denote the damage-sensitive parameters for the reference and test datasets, respectively. This study formulates the hypotheses according to the following conditions.

- The damage-sensitive parameters for the null hypothesis $\mathcal{H}_0$ are consistent between the reference and test datasets, i.e., $\mathbf{\Theta}_{\mathrm{feat}}^{\mathrm{r}} = \mathbf{\Theta}_{\mathrm{feat}}^{\mathrm{t}}$.
- The damage-sensitive parameters for the alternative hypothesis $\mathcal{H}_1$ differ between the reference and test datasets, i.e., $\mathbf{\Theta}_{\mathrm{feat}}^{\mathrm{r}} \neq \mathbf{\Theta}_{\mathrm{feat}}^{\mathrm{t}}$.
- The other parameters of both hypotheses are consistent between the reference and test datasets.

This method adopts parameters $\mathbf{\Theta} = \left\{\widetilde{\mathbf{W}}', \mathbf{\Sigma}\right\}$ and damage sensitive parameters $\mathbf{\Theta}_{\mathrm{feat}} = \widetilde{\mathbf{W}}'_{\mathbf{I},\boldsymbol{i}}$. Under the null hypothesis, we assume that no parameter differs between the reference and test datasets. Therefore, the PDF of the parameters for the null hypothesis is identical to Equation 22, i.e. $p\left(\widetilde{\mathbf{W}}', \mathbf{\Sigma}|\mathcal{H}_0\right) = p\left(\widetilde{\mathbf{W}}', \mathbf{\Sigma}|\mathcal{D}_{\mathrm{r}}\right)$. Under the alternative hypothesis, damage-sensitive parameters for the i-th mode $\widetilde{\mathbf{W}}'_{\mathbf{I},\boldsymbol{i}}$ are altered from the reference dataset and remain unknown until the test dataset is observed. The alternative hypothesis adopts the following PDF with broad variances.

$$\mathrm{p}\left(\widetilde{\mathbf{W}}'^{\mathbf{t}}_{\mathbf{I},\boldsymbol{i}}|\mathbf{\Sigma}, \mathcal{H}_1\right) = \prod\nolimits_{i=1}^{q} \mathcal{MN}\left(\widetilde{\mathbf{W}}'_{\mathbf{I},i}|\mathbf{0}, \alpha^{-1}\mathbf{\Sigma}\right) \tag{25}$$

Here, 0 is adopted as the mean value of the damage-sensitive parameters $\widetilde{\mathbf{W}}_{\mathbf{I},i}^{\prime\mathbf{t}}$ to avoid bias derived from the reference dataset. α is a coefficient that approximately maximizes the alternative hypothesis, assuming the modal properties remain unchanged. This study adopts the following coefficient.

$$\alpha := \frac{2m}{\mathrm{trace}\left[\widetilde{\mathbf{M}}_{\mathbf{I},\mathbf{i}}^{\mathbf{T}}\widehat{\mathbf{\Sigma}}^{-1}\widetilde{\mathbf{M}}_{\mathbf{I},\mathbf{i}}\right]} \tag{26}$$

The Bayes factor is defined as

$$\boldsymbol{B} = \frac{\int p(\mathcal{D}_{\mathrm{t}}|\boldsymbol{\Theta})p(\boldsymbol{\Theta}|\mathcal{H}_1)d\boldsymbol{\Theta}}{\int p(\mathcal{D}_{\mathrm{t}}|\boldsymbol{\Theta})p(\boldsymbol{\Theta}|\mathcal{H}_0)d\boldsymbol{\Theta}} \tag{27}$$

This study adopts the normalized log-scaled Bayes factor as the damage indicator

$$DI = \frac{2}{m(n_t - p)}\ln \boldsymbol{B} \tag{28}$$

where n_t stands for data length of $\mathcal{D}_{\mathrm{t}}$. If $DI > 0$ is satisfied, the i-th mode in the state space is altered. How to calculate $\ln \boldsymbol{B}$ is shown in (Goi & Kim, 2023).

3 Case Study

This study provides a case study for a simply-supported truss bridge to assess the feasibility of the proposed method. The schematic outline of the structure and the sensor deployment are shown in Figure 1. Eight uniaxial accelerometers were installed on the bridge deck to measure vertical vibrations. The truss members were severed in the field experiment. This study applies anomaly detection for the scenario in which half-cut and full-cut damages were applied to a vertical truss member at mid-span, as shown in Figure 2. Further details of the experiments are shown in (Kim et al., 2021).

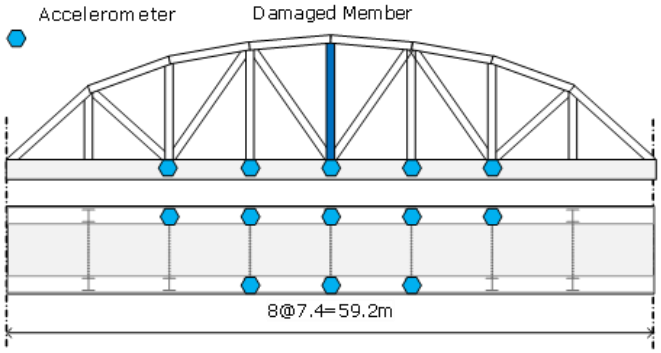

Figure 1. Schematic outline of the target bridge

Figure 2. Damaged members

3.1 *Training*

For the reference dataset, the vehicle passed over the deck at three speeds: 30 km/h, 40 km/h, and 50 km/h. The data measured at different vehicle speeds were mixed into the reference dataset to increase training robustness. The vehicle passed 11 times at 30 km/h, 10 times at 40 km/h, and 5 times at 50 km/h. From the reference dataset, the AR order is automatically determined to be p=135. The differential SN ratio in Equation 20 is shown in Figure 3. This diagram indicates that the signal from the 14th and higher-order modal responses has less power than the noise term in the VAR model. Therefore, this case study uses the 13-DOF system for anomaly detection.

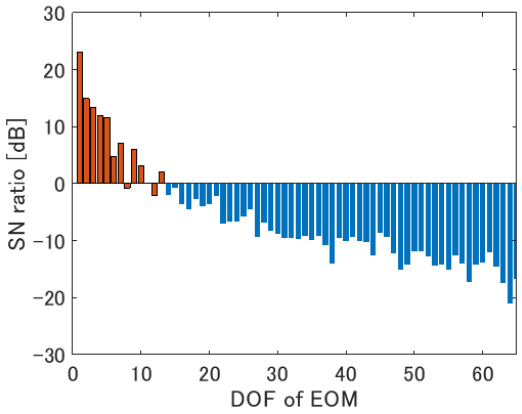

Figure 3. Differential SN ratios

In Figure 4, black lines represent the PSD of the raw data. Here, each black line shows the periodogram of the acceleration measured by each accelerometer and represents the average value from the 26 vehicle loading tests. The blue line represents PSD estimators from the learned VAR model. Figure 4 indicates that the learned 135-order VAR model fits the raw data well. Note that the BIC helps avoid overfitting caused by too-high-order VAR models. Figure 4 also shows the modal frequencies estimated by SSI-COV using the 13-DOF state-space model. These results show that most SSI-COV estimators correspond to peaks in the PSD curves. Figure 5 shows several examples of SSI-COV estimators of mode shapes. The two lines show the mode shapes at the deck's two edges. Therefore, Modes 1, 4, and 5, respectively, represent bending modes. Modes 2 and 3 exhibit asymmetric modal deformation, which may be due to lateral or torsional modes. Mode 6 seems to be the second torsional mode.

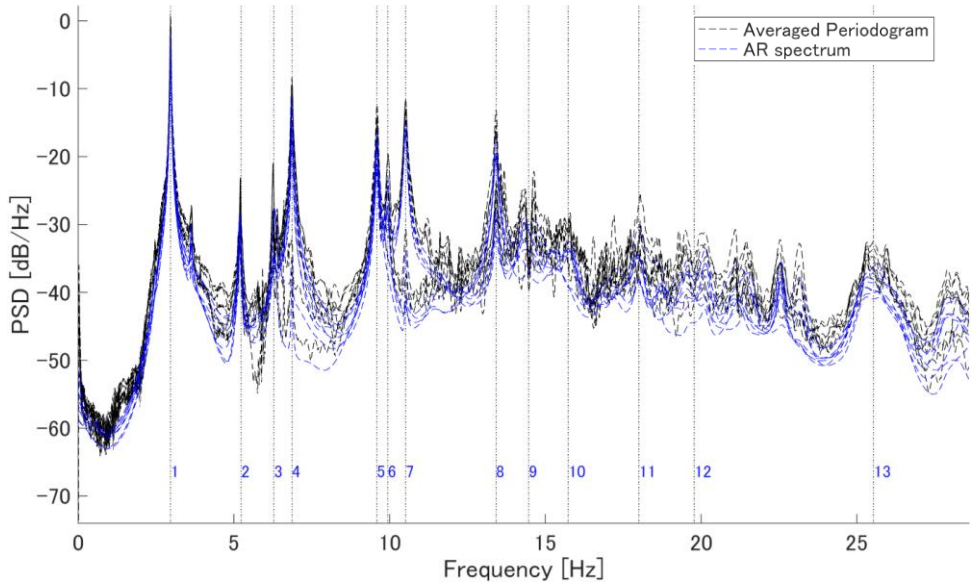

Figure 4. The trained spectrum and extracted modal frequencies

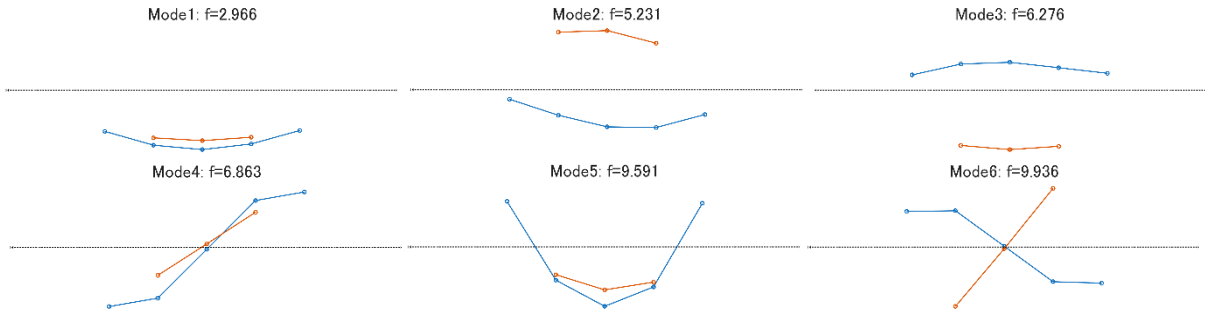

Figure 5. Example of estimated mode shapes

3.2 *Testing*

Damage indicators defined in Equation 28 are calculated for each of the 13 modes. Figure 6 shows the damage indicators for the half-cut damage. The mode numbers in the x-axis correspond to the numbers in Figure 4. Black circles are the damage indicators from the leave-one-out cross-validation (CV) on the reference dataset. Each sample is calculated from a time series of each vehicle's loadings. These results represent data without damage, so it is expected that $DI < 0$ holds for CV samples. Red crosses indicate damage in the test dataset. If the modal response involves an anomaly, then $DI > 0$ is expected. Therefore, this study proposes the following threshold for anomaly detection.

$$(\text{median}[DI \text{ of CV Samples}] < 0) \text{and } (0 < \text{median}[DI \text{ of Test Samples}]) \tag{29}$$

Figure 6 also shows the medians for the CV samples and the test samples. Equation 29 enables distinguishing which mode involves an anomaly in the test dataset. In Figure 5, Equation 29 indicates that Modes 1, 4, 7, 8, 10, and 11 are positively altered modes. The higher modes, i.e., Modes 12 and 13, are unstable, and the median of the CV samples exceeds the threshold 0. Figure 7 shows the damage indicators for full-cut damage in the same way as Figure 6. The y-axis scale is altered from Figure 6. These results indicate that Modes 1 and 2 have a much larger anomaly than the others. Equation 29 indicates that Modes 3, 4, 5, 7, 8, 10, and 11 are also altered. This result suggests the proposed damage indicator also indicates the severity of the changes in each mode. However, further investigation is needed to scale the severity.

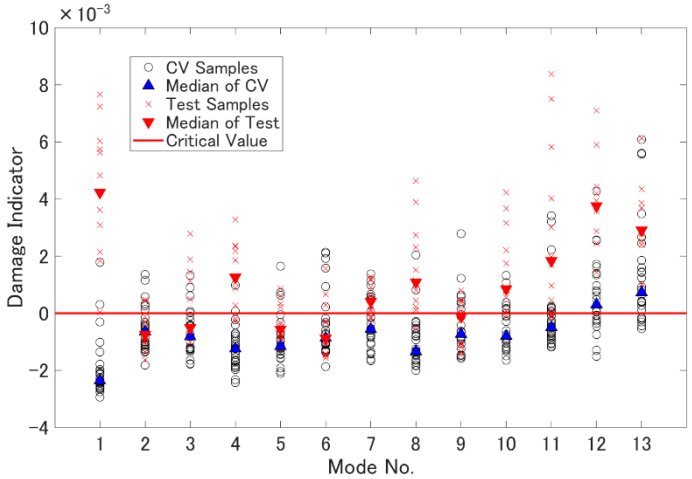

Figure 6. Damage indicators for half-cut damage

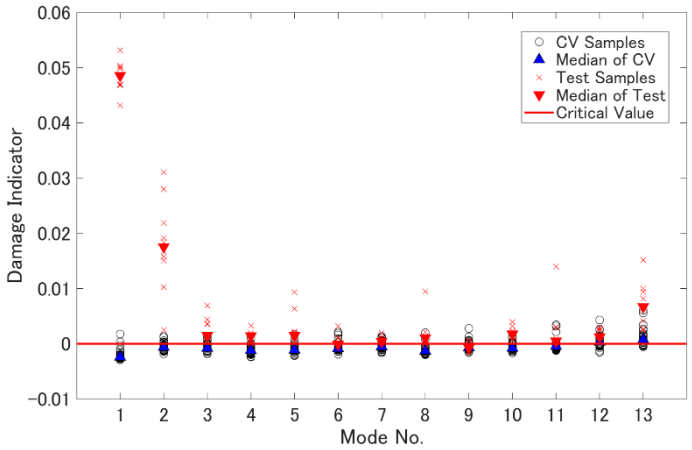

Figure 7. Damage indicators for full-cut damage

4 Conclusion

To screen numerous bridges, this study proposed a two-step anomaly-detection approach to detect changes in modal properties. In this method, Bayesian inference is applied to a vector autoregressive (VAR) model to represent bridge vibration. Covariance-driven stochastic subspace identification (SSI-COV) is applied to extract a parametric subspace corresponding to each mode from the VAR model. Bayesian hypothesis testing quantifies anomalies in a subspace extracted with SSI-COV. The proposed method enables the direct detection of anomalies in each modal property from measured acceleration. The autoregressive order and the degree of freedom (DOF) of the equation on motion are automatically adjusted with the Bayesian information criterion and signal-to-noise ratio.

A field experiment on a truss bridge with severed members was examined as a case study. The training step showed that the proposed feature extraction method is consistent with existing modal identification methods. The testing step suggests distinguishing altered modes from the multi-DOF system. Furthermore, the proposed damage indicator suggests the severity of the changes in each mode. Further investigation will be conducted to determine the relationship between the proposed damage indicator and the damage sensitivity of each mode.

Acknowledgments

The Japanese Society partly sponsored this study for Early Career Scientists under Project No. 23K13394. The financial support is gratefully acknowledged.

References

Goi, Y. and Kim, C.W., Bridge Damage Detection Using Ambient Loads by Bayesian Hypothesis Testing for a Parametric Subspace of an Autoregressive Model, *Structural Control and Health Monitoring*, 2023, 7986061, 2023.

Kim, C.W., Zhang, F.L., Chang, K.C., McGetric, P., and Goi, Y., Old ADA Bridge-damage vibration data, *Mendeley Data*. V2, 2021.

Rabi, R.R., Vailati, M., and Monti, G., Effectiveness of Vibration-Based Techniques for Damage Localization and Lifetime Prediction in Structural Health Monitoring of Bridges: A Comprehensive Review. *Buildings*, 14 (4), 1183, 2024.

van Overschee, P. and De Moor, B, Subspace Identification for Linear Systems, *Kluwer Academic Publishers*, 1996